Spherical orbits in Kerr spacetime

O. Kopáček[1,2] V. Karas[1]

[1]Astronomical Institute
Academy of Sciences of the Czech Republic

[2]Department of Physics
Technical University of Liberec

23rd September 2024, Czech LISA meeting, Prague

Spherical orbits

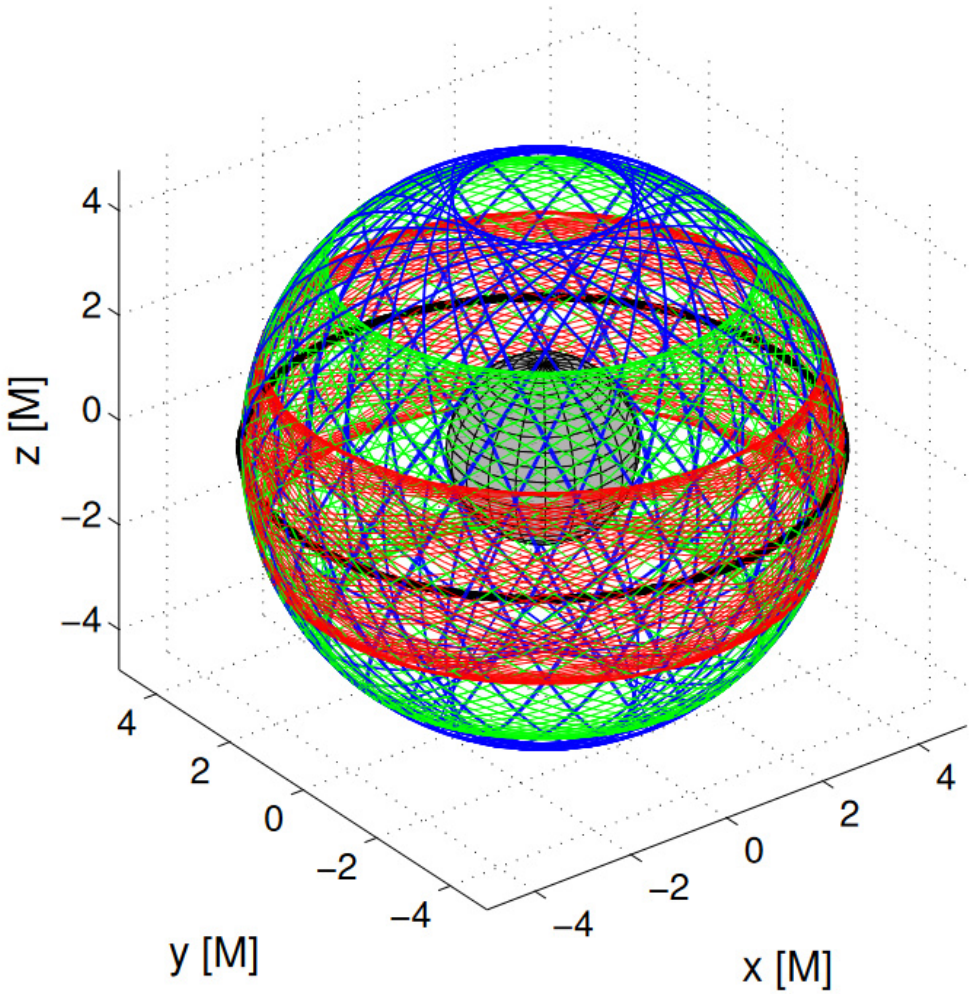

Figure 1. Example of a set of spherical orbits launched at the radius $r = 5$ from the equatorial plane of a Kerr black hole ($a = 0.8$) differing solely by the value of Carter constant Q which specifies the initial value of $p_\theta = Q^{1/2}$. In particular, we compare the trajectories with $Q = 0$ (black circular orbit), $Q = 1$ (red), $Q^{1/2} = 2$ (green) and $Q^{1/2} = 3$ (blue).

Polar orbits

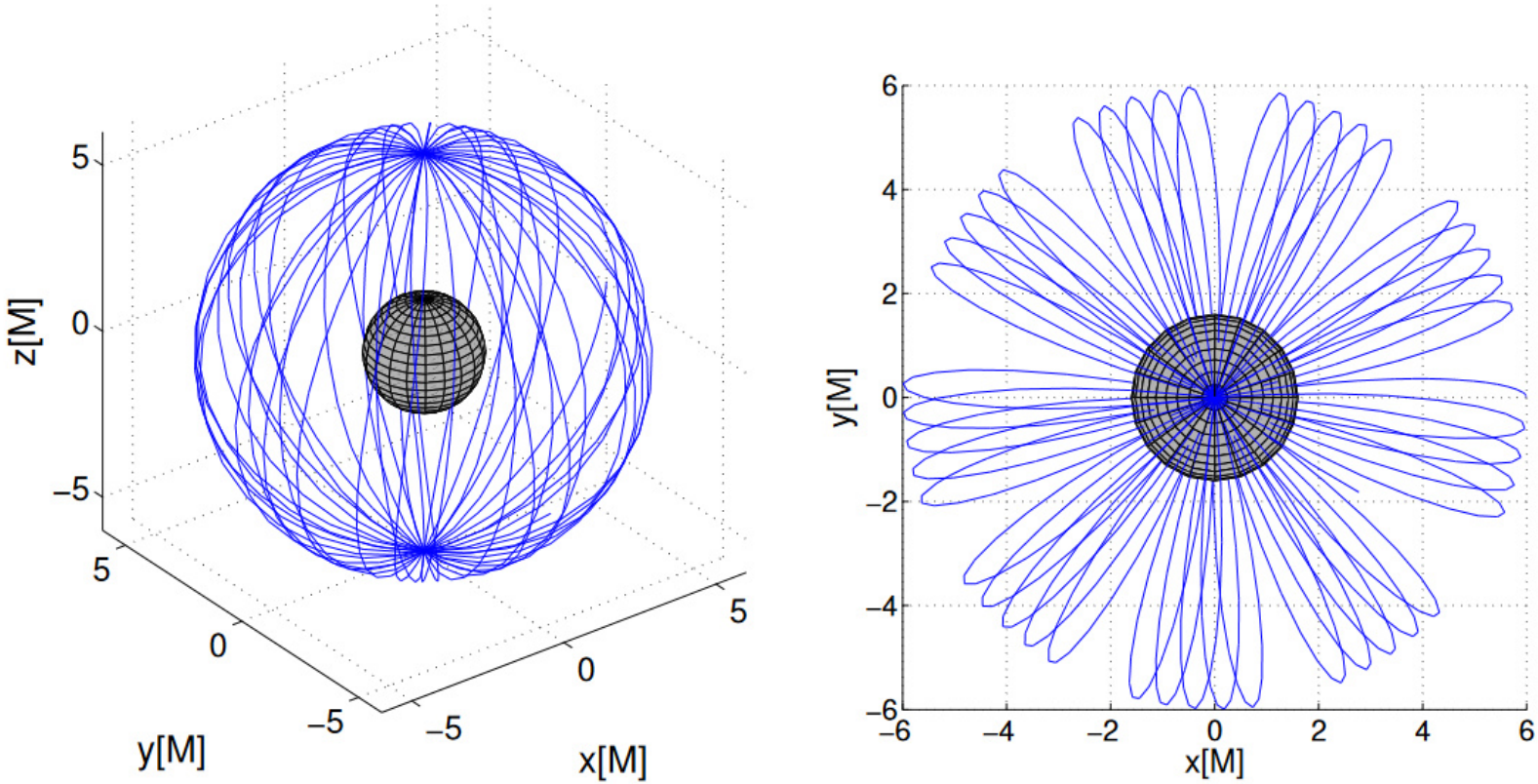

Figure 2. Stable polar orbit around Kerr black hole ($a = 0.8$) with radius $r = 6$.

History

- Kerr, R. P. (**1963**), Gravitational Field of a Spinning Mass as an Example of Algebraically Special Metrics, Physical Review Letters, 11, 237.
- Newman, E. T., Couch, E., Chinnapared, K., Exton, A., Prakash, A., & Torrence, R. (**1965**), Metric of a Rotating, Charged Mass, Journal of Mathematical Physics, 6, 918.
- Carter, B. (**1968**), Global Structure of the Kerr Family of Gravitational Fields, Physical Review, 174, 1559.
- Wilkins, D. C. (**1972**), Bound Geodesics in the Kerr Metric, Physical Review D, 5, 814.
- Bardeen, J. M., Press, W. H., & Teukolsky, S. A. (**1972**), Rotating Black Holes: Locally Nonrotating Frames, Energy Extraction, and Scalar Synchrotron Radiation, The Astrophysical Journal, 178, 347.
- Goldstein, H. (**1974**), Numerical calculation of bound geodesics in the Kerr metric, Zeitschrift fur Physik, 271, 275.
- Dymnikova, I. G. (**1986**), REVIEWS OF TOPICAL PROBLEMS: Motion of particles and photons in the gravitational field of a rotating body (In memory of Vladimir Afanas'evich Ruban), Soviet Physics Uspekhi, 29, 215.
- Shakura, N. I. (**1987**), Geodesics in a Kerr Metric, Soviet Astronomy Letters, 13, 99.
- Rana, P., & Mangalam, A. (**2019**), Astrophysically relevant bound trajectories around a Kerr black hole, Classical and Quantum Gravity, 36, 045009.
- Teo, E. (**2021**), Spherical orbits around a Kerr black hole, General Relativity and Gravitation, 53, 10.

components of the particle's 4-momentum at some instant, these conserved quantities are

$$E = -p_t = \text{total energy},$$
$$L = p_\varphi = \text{component of angular momentum parallel to symmetry axis},$$
$$Q = p_\theta^2 + \cos^2\theta[a^2(\mu^2 - p_t^2) + p_\varphi^2/\sin^2\theta]. \tag{2.8}$$

Here μ is the rest mass of the particle ($\mu = 0$ for photons), which is a trivial fourth constant of the motion. Note that $Q = 0$ is a necessary and sufficient condition for motion initially in the equatorial plane to remain in the equatorial plane for all time. Any orbit which crosses the equatorial plane has $Q > 0$. When $a = 0$, $Q + p_\varphi^2$ is the square of the total angular momentum. By solving equation (2.8) for the p_μ's and thence the p^μ's, one obtains equations governing the orbital trajectory,

$$\Sigma\frac{dr}{d\lambda} = \pm(V_r)^{1/2}, \tag{2.9a}$$

$$\Sigma\frac{d\theta}{d\lambda} = \pm(V_\theta)^{1/2}, \tag{2.9b}$$

$$\Sigma\frac{d\varphi}{d\lambda} = -(aE - L/\sin^2\theta) + aT/\Delta, \tag{2.9c}$$

$$\Sigma\frac{dt}{d\lambda} = -a(aE\sin^2\theta - L) + (r^2 + a^2)T/\Delta. \tag{2.9d}$$

Here λ is related to the particle's proper time by $\lambda = \tau/\mu$, and is an affine parameter in the case $\mu \to 0$, and

$$T \equiv E(r^2 + a^2) - La,$$
$$V_r \equiv T^2 - \Delta[\mu^2 r^2 + (L - aE)^2 + Q],$$
$$V_\theta \equiv Q - \cos^2\theta[a^2(\mu^2 - E^2) + L^2/\sin^2\theta]. \tag{2.10}$$

Without loss of generality one is free to take $\mu = 1$ for particles and $\mu = 0$ for photons, in equations (2.8), (2.9), (2.10). (For particles this merely renormalizes E, L, and Q to a "per unit rest mass" basis.) V_r and V_θ are "effective potentials" governing particle motions in r and θ. Notice that V_r is a function of r only, V_θ is a function of θ only, and consequently equations (2.9a) and (2.9b) form a decoupled pair. Also, it is not difficult to show (Wilkins 1972) that if $E/\mu < 1$ the orbit is bound (does not reach $r = \infty$), while all orbits with $E/\mu > 1$ are unbound except for a "measure-zero" set of unstable orbits.

The single most important class of orbits are the circular orbits in the equatorial plane. For a circular orbit at some radius r, $dr/d\lambda$ must vanish both instantaneously and at all subsequent times (orbit at a perpetual turning point). Equation (2.9a) then gives the conditions

$$V_r(r) = 0, \qquad V_r'(r) = 0. \tag{2.11}$$

These equations can be solved simultaneously for E and L to give

$$E/\mu = \frac{r^{3/2} - 2Mr^{1/2} \pm aM^{1/2}}{r^{3/4}(r^{3/2} - 3Mr^{1/2} \pm 2aM^{1/2})^{1/2}}, \tag{2.12}$$

$$L/\mu = \frac{\pm M^{1/2}(r^2 \mp 2aM^{1/2}r^{1/2} + a^2)}{r^{3/4}(r^{3/2} - 3Mr^{1/2} \pm 2aM^{1/2})^{1/2}}. \tag{2.13}$$

In these and all subsequent formulae, the upper sign refers to direct orbits (i.e., corotating with $L > 0$), while the lower sign refers to retrograde orbits (counter-rotating with $L < 0$). For an extreme-rotating black hole, $a = M$, equations (2.12) and (2.13) simplify somewhat,

$$E/\mu = \frac{r \pm M^{1/2}r^{1/2} - M}{r^{3/4}(r^{1/2} \pm 2M^{1/2})^{1/2}}, \qquad \text{for } a = M; \tag{2.14}$$

$$L/\mu = \frac{\pm M(r^{3/2} \pm M^{1/2}r + Mr^{1/2} \mp M^{3/2})}{r^{3/4}(r^{1/2} \pm 2M^{1/2})^{1/2}}, \qquad \text{for } a = M. \tag{2.15}$$

The coordinate angular velocity of a circular orbit is

$$\Omega \equiv d\varphi/dt = \pm M^{1/2}/(r^{3/2} \pm aM^{1/2}). \tag{2.16}$$

Circular orbits do not exist for all values of r. The denominator of equations (2.12) and (2.13) is real only if

$$r^{3/2} - 3Mr^{1/2} \pm 2aM^{1/2} \geq 0. \tag{2.17}$$

The limiting case of equality gives an orbit with infinite energy per unit rest mass, i.e., a photon orbit. This photon orbit is the innermost boundary of the circular orbits for particles; it occurs at the root of (2.17),

$$r = r_{\rm ph} \equiv 2M\{1 + \cos[\tfrac{2}{3}\cos^{-1}(\mp a/M)]\}. \tag{2.18}$$

For $a = 0$, $r_{\rm ph} = 3M$, while for $a = M$, $r_{\rm ph} = M$ (direct) or $4M$ (retrograde).

For $r > r_{\rm ph}$ not all circular orbits are bound. An unbound circular orbit is one with $E/\mu > 1$. Given an infinitesimal outward perturbation, a particle in such an orbit will escape to infinity on an asymptotically hyperbolic trajectory. The unbound circular orbits are circular in geometry but hyperbolic in energetics, and they are all unstable. Bound circular orbits exist for $r > r_{\rm mb}$, where $r_{\rm mb}$ is the radius of the marginally bound ("parabolic") circular orbit with $E/\mu = 1$,

$$r_{\rm mb} = 2M \mp a + 2M^{1/2}(M \mp a)^{1/2}. \tag{2.19}$$

Note also that $r_{\rm mb}$ is the minimum perihelion of all parabolic ($E/\mu = 1$) orbits. In astrophysical problems, particle infall from infinity is very nearly parabolic, since the velocities of matter at infinity satisfy $v \ll c$. Any parabolic trajectory which penetrates to $r < r_{\rm mb}$ must plunge directly into the black hole. For $a = 0$, $r_{\rm mb} = 4M$; for $a = M$, $r_{\rm mb} = M$ (direct) or $5.83M$ (retrograde).

Even the bound circular orbits are not all stable. Stability requires that $V_r''(r) \leq 0$, which yields the three equivalent conditions

$$1 - (E/\mu)^2 \geq \tfrac{2}{3}(M/r),$$
$$r^2 - 6Mr \pm 8aM^{1/2}r^{1/2} - 3a^2 \geq 0,$$

or

$$r \geq r_{\rm ms}, \tag{2.20}$$

where $r_{\rm ms}$ is the radius of the marginally stable orbit,

$$r_{\rm ms} = M\{3 + Z_2 \mp [(3 - Z_1)(3 + Z_1 + 2Z_2)]^{1/2}\},$$
$$Z_1 \equiv 1 + (1 - a^2/M^2)^{1/3}[(1 + a/M)^{1/3} + (1 - a/M)^{1/3}],$$
$$Z_2 \equiv (3a^2/M^2 + Z_1^2)^{1/2}. \tag{2.21}$$

For $a = 0$, $r_{\rm ms} = 6M$; for $a = M$, $r_{\rm ms} = M$ (direct) or $9M$ (retrograde). Figure 1

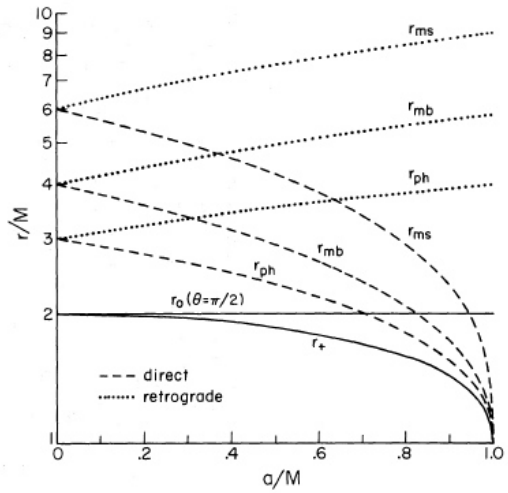

FIG. 1.—Radii of circular, equatorial orbits around a rotating black hole of mass M, as functions of the hole's specific angular momentum a. Dashed and dotted curves (for direct and retrograde orbits) plot the Boyer-Lindquist coordinate radius of the innermost stable (ms), innermost bound (mb), and photon (ph) orbits. Solid curves indicate the event horizon (r_+) and the equatorial boundary of the ergosphere (r_0).

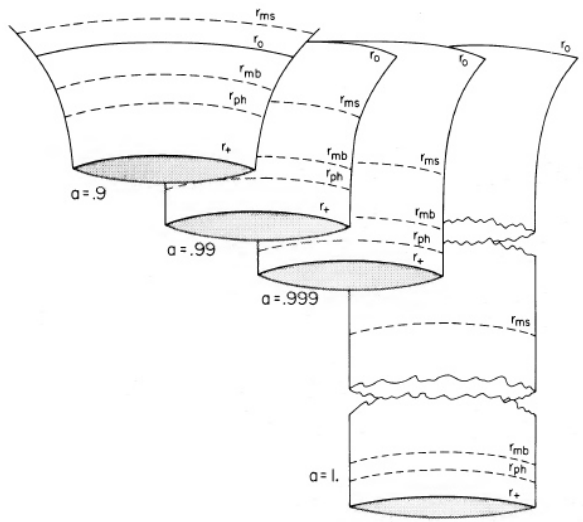

FIG. 2.—Embedding diagrams of the "plane" $\theta = \pi/2$, t = constant, for rotating black holes with near-maximum angular momentum. Here a denotes the hole's angular momentum in units of M. The Boyer-Lindquist radial coordinate r determines only the circumference of the "tube." When $a \to M$, the orbits at r_{ms}, r_{mb}, and r_{ph} all have the same circumference and coordinate radius, although—as the embedding diagram shows clearly—they are in fact distinct.

ISCO of charged particles in Kerr-Newman spacetime

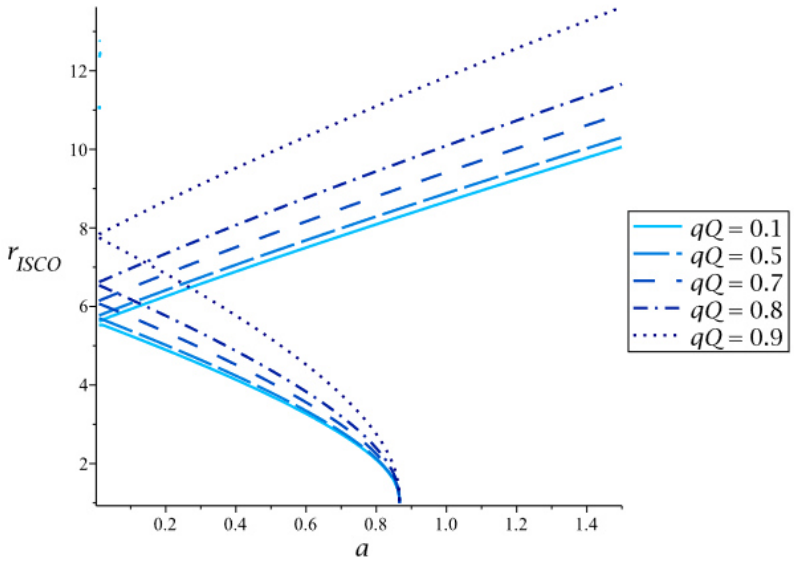

- Schroven, K., & Grunau, S. (**2021**), Innermost stable circular orbit of charged particles in Reissner-Nordström, Kerr-Newman, and Kerr-Sen spacetimes, Physical Review D, 103, 024016.
  "The radius of the ISCO increases with an increasing particle-black hole charge product $|qQ|$ in the case of attractive Coulomb interaction $qQ < 0$. For the repulsive Coulomb interaction, the ISCO radius first decreases to a minimum and then increases again, until it diverges as the charge product approaches one."
- Hackmann, E., & Xu, H. (**2013**), Charged particle motion in Kerr-Newmann space-times, Physical Review D, 87, 124030.

Spherical orbits parametrized by inclination angle

Energy and angular momentum of the spherical orbits may be expressed explicitly as a function of radius, spin, and latitudinal turning point $\theta_\star$ (Shakura, 1987):

$$E = \frac{1 - \frac{2r}{\Sigma_\star} \pm \frac{aq_\star}{\Sigma_\star\sqrt{r}} \sin\theta_\star}{\left(1 - \frac{3r}{\Sigma_\star} \pm \frac{2aq_\star}{\Sigma_\star\sqrt{r}} \sin\theta_\star + \frac{a^2}{\Sigma_\star r}\cos^2\theta_\star\right)^{1/2}},$$

$$L = \frac{\pm\frac{q_\star(r^2+a^2)}{\Sigma_\star\sqrt{r}} \sin\theta_\star - \frac{2ar}{\Sigma_\star}\sin^2\theta_\star}{\left(1 - \frac{3r}{\Sigma_\star} \pm \frac{2aq_\star}{\Sigma_\star\sqrt{r}} \sin\theta_\star + \frac{a^2}{\Sigma_\star r}\cos^2\theta_\star\right)^{1/2}},$$

where $\Sigma_\star = r^2 + a^2\cos^2\theta_\star$ and $q_\star = (r^2 - a^2\cos^2\theta_\star)^{1/2}$. Upper signs correspond to co-rotating (direct) orbits while the lower signs are valid for counter-rotating orbits. With the inclination $\theta_\star = \pi/2$ the above expressions reduce to familiar formulas for circular (Keplerian) orbits in the equatorial plane.

Spherical orbits parametrized by Carter constant

Alternatively to the parameterization by the value of the turning point $\theta_\star$, it is also possible to parameterize the integrals of motion E and L by the Carter constant Q (Teo, 2021):

$$
\begin{aligned}
E &= \frac{r^3\left(r-2\right)-a\left(aQ\mp\sqrt{\Upsilon}\right)}{r^2\sqrt{r^3\left(r-3\right)-2a\left(aQ\mp\sqrt{\Upsilon}\right)}}, \\
L &= -\frac{2ar^3+\left(r^2+a^2\right)\left(aQ\mp\sqrt{\Upsilon}\right)}{r^2\sqrt{r^3\left(r-3\right)-2a\left(aQ\mp\sqrt{\Upsilon}\right)}},
\end{aligned}
$$

where $\Upsilon = r^5 - Q(r-3)r^3 + a^2Q^2$. Submitting $Q = 0$, we may again verify that the above formulas reduce to expressions for circular orbits.

Properties of spherical orbits

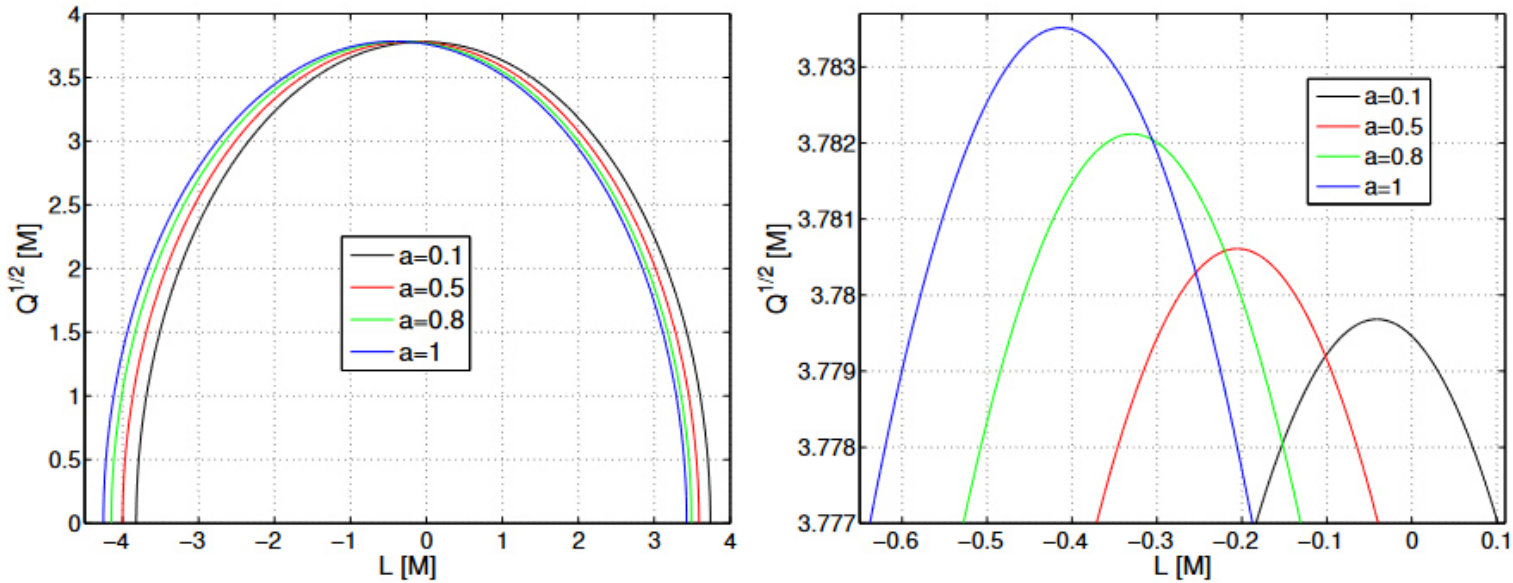

Figure 3. Square root of the Carter constant of spherical orbits at $r = 10$ as a function of angular momentum L for several values of spin. In the right panel, we zoom the section of the left plot around maximal values.

ISSO and MBSO

For spherical orbits, the radius $r = r_{ms}$ of Innermost Stable Spherical Orbit (ISSO), and the related radius $r = r_{mb}$ of the Marginally Bound Spherical Orbit (MBSO) are given implicitly by the following algebraic relations (Rana, 2019):

$$r_{ms}^9 - 12r_{ms}^8 - 6a^2 r_{ms}^7 + 36r_{ms}^7 + 8a^2 Q r_{ms}^6 - 28a^2 r_{ms}^6 - 24a^2 Q r_{ms}^5 + 9a^4 r_{ms}^5 - 24a^4 Q r_{ms}^4 + 48a^2 Q r_{ms}^4 + 16a^4 Q^2 r_{ms}^3 - 8a^4 Q r_{ms}^3 - 48a^4 Q^2 r_{ms}^2 + 48a^4 Q^2 r_{ms} - 16a^6 Q^2 = 0,$$

and

$$r_{mb}^8 - 8r_{mb}^7 - 2a^2 r_{mb}^6 + 16r_{mb}^6 + 2a^2 Q r_{mb}^5 - 8a^2 r_{mb}^5 - 6a^2 Q r_{mb}^4 + a^4 r_{mb}^4 - 2a^4 Q r_{mb}^3 + 8a^2 Q r_{mb}^3 + a^4 Q^2 r_{mb}^2 - 2a^4 Q r_{mb}^2 - 2a^4 Q^2 r_{mb} + a^4 Q^2 = 0.$$

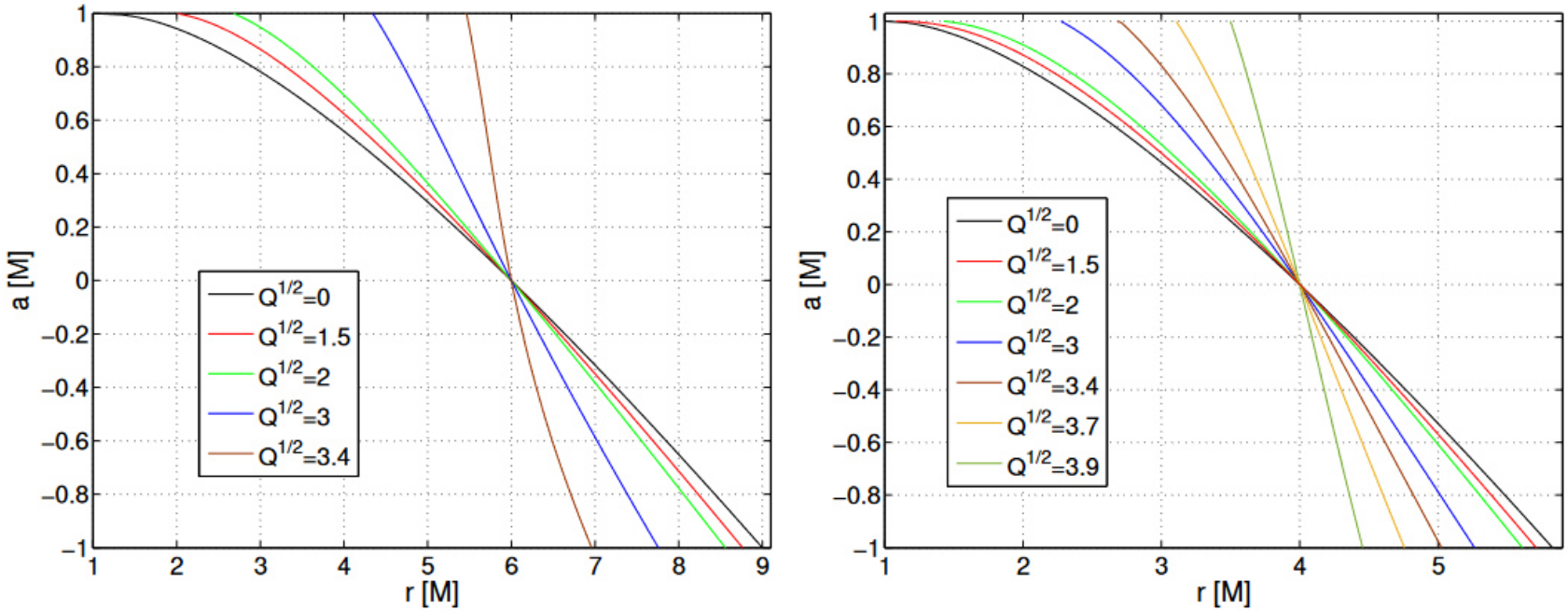

Figure 4. Locations of the innermost stable spherical orbits (left panel) and marginally bound spherical orbits (right panel) with different values of the Carter constant and spin. On the vertical axis, parameter $a[M] \equiv \sigma a$ is shown, where a is the Kerr spin parameter, for which $a \geq 0$ is assumed throughout the paper, and $\sigma = \pm 1$ is a switch that distinguishes prograde vs. retrograde motion. Positive values ($\sigma = 1$) correspond to orbits co-rotating with the black hole, while negative values ($\sigma = -1$) are for the counter-rotating orbits. These graphs generalize the well-known dependence of the equatorial ISCO radius to the case of orbits inclined with respect to the equatorial plane.

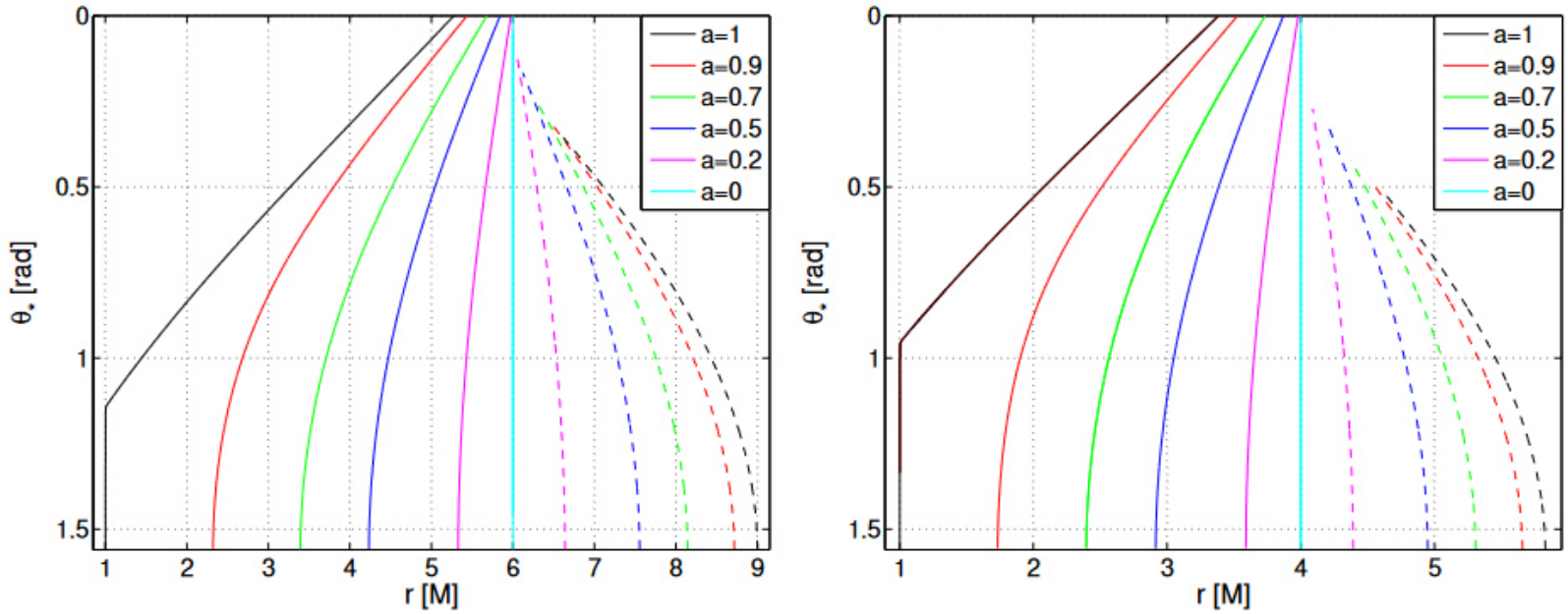

Figure 5. Locations of the innermost stable spherical orbits (left panel) and marginally bound spherical orbits (right panel) with respect to the inclination $\theta_\star$ for different values of the spin parameter. The meaning of $\theta_\star$ is the angular distance of the latitudinal turning point from the zenith or nadir, respectively (see the main text for further details). Dashed lines correspond to the counter-rotating spherical orbits. We notice that the vertical axes of the plots are inverted, i.e., their lower edges ($\theta_\star = \pi/2$) correspond to circular orbits in the equatorial plane, while polar orbits with $\theta_\star = 0$ are found on the upper edges.

ISPO and MBPO

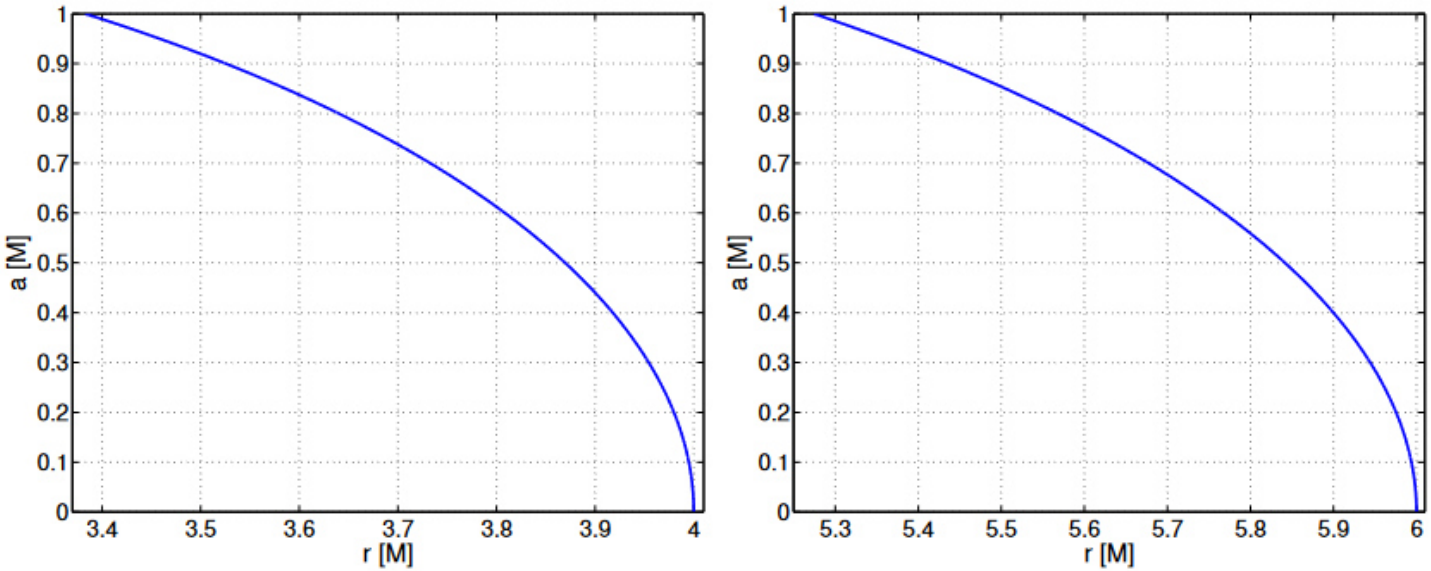

Figure 8. Left panel: radii of marginally bound polar orbits (MBPO). Right panel: radii of innermost stable polar orbits (ISPO).

Stable spherical orbits above ISSO

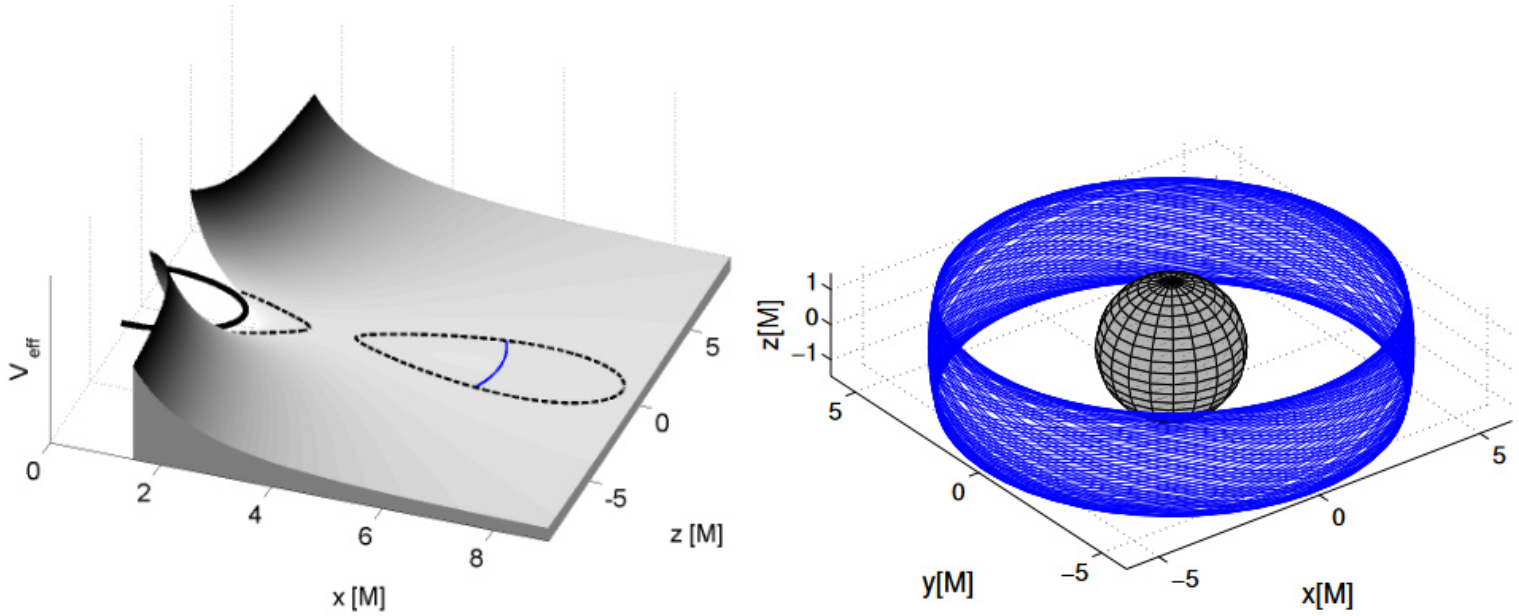

Figure 9. Example of a stable spherical orbit above ISSO. The left panel shows the effective potential Eq. (6) of the particle with angular momentum given by Eq. (14) while the equipotential curve of corresponding energy given by Eq. (13) is marked by the dashed black line. The solid black line marks the horizon of the black hole. The blue curve shows the projected trajectory. In the right panel, the same trajectory is shown in three dimensions with the horizon marked by the grey sphere. Following parameters were employed: $r_0 = 6.5$, $Q^{1/2} = 0.75$ and $a = 0.5$.

Unstable spherical orbits between MBSO and ISSO

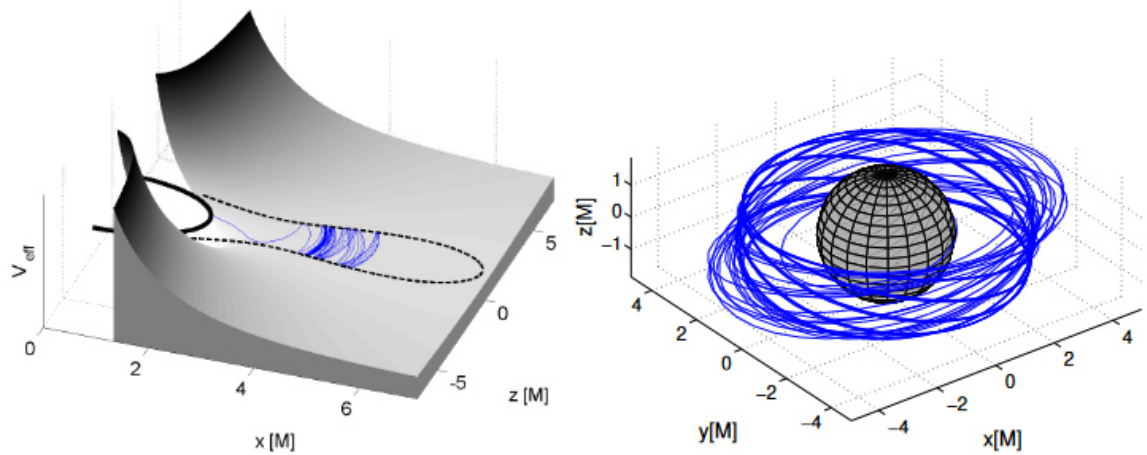

Figure 10. Example of an unstable plunging spherical orbit launched below ISSO. Following parameters were employed: $r_0 = 4$, $Q^{1/2} = 0.75$ and $a = 0.5$.

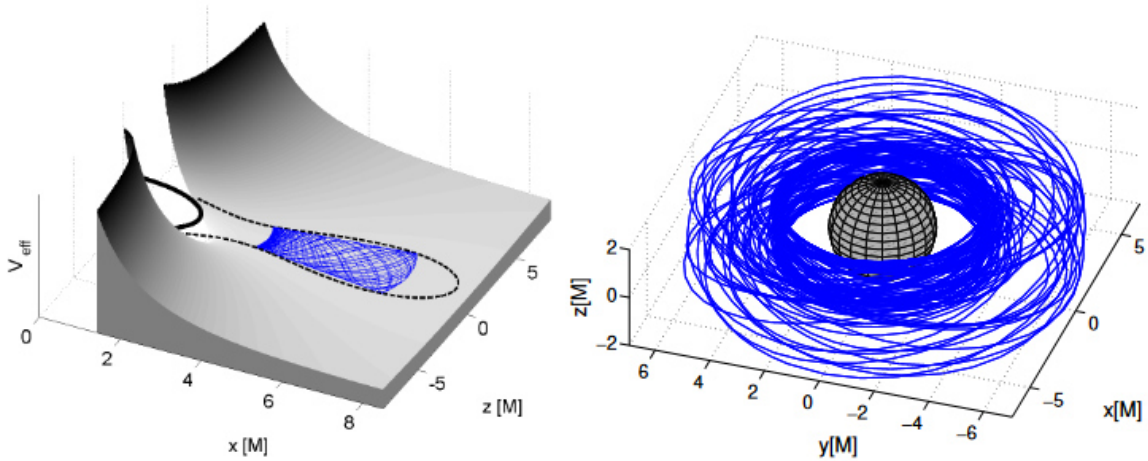

Figure 11. Example of an unstable spherical orbit launched below ISSO which evolves into quasiperiodic radially bounded orbit due to numerical perturbation resulting from integration errors. Following parameters were employed: $r_0 = 3.6$, $Q^{1/2} = 0.75$ and $a = 0.5$.

Dynamics between MBSO and ISSO

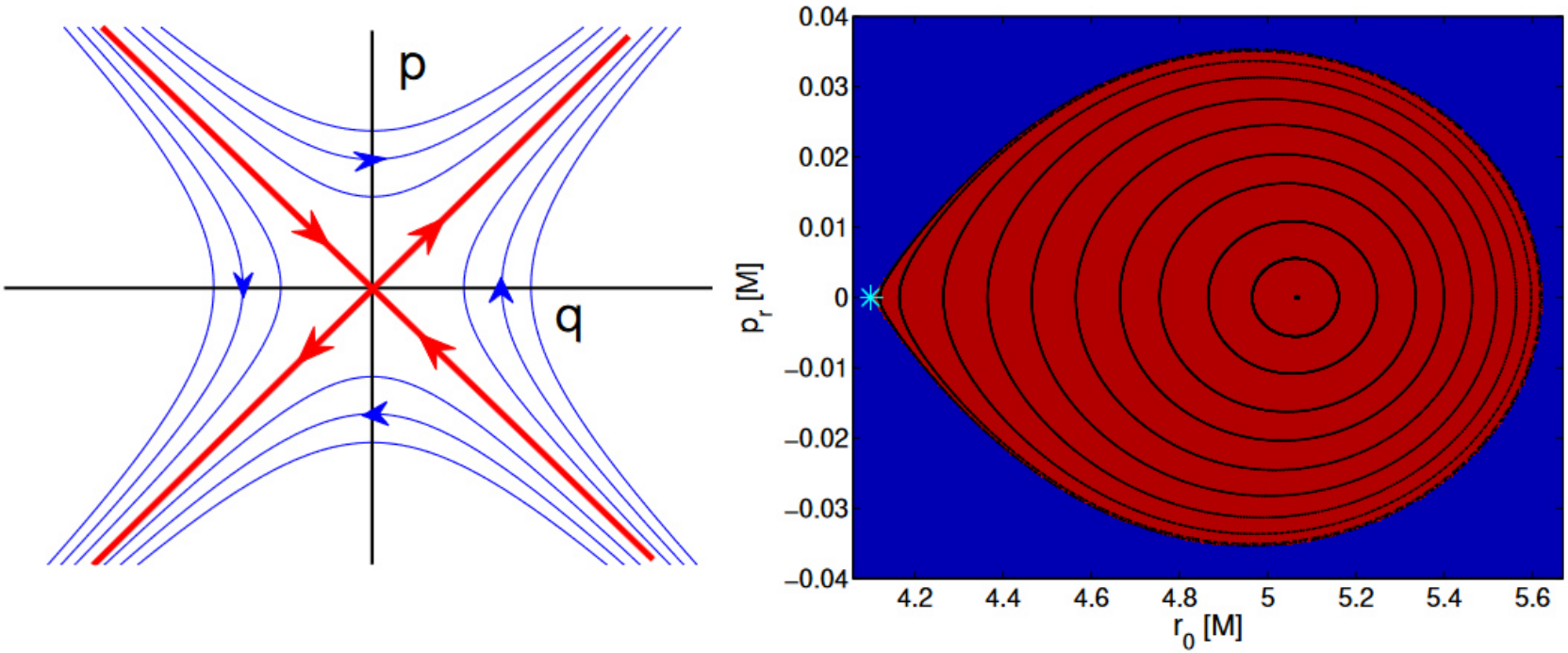

Figure 16. Left panel: a sketch of the dynamics in the neighborhood of a saddle-type unstable hyperbolic fixed point in a two-dimensional dynamical system with phase-space coordinates $(q, p) = (0, 0)$. Separatrix (red) and flow lines (blue) in different phase-space regions are shown. Right panel: example of actual dynamics near an unstable spherical orbit between MBSO and ISSO radii with parameters $r_0 = 4.1$, $Q^{1/2} = 3$ and $a = 0.9$ (light-blue asterisk). The blue region corresponds to plunging orbits, red region consists of radially bounded quasiperiodic orbits. Poincaré surface of section (taken at $\theta = \pi/2$ for $\dot{\theta} > 0$) with canonical coordinates (r, p_r) of several quasiperiodic trajectories within the bound region differing in initial radii is shown with black color.

Dynamics between MBSO and ISSO

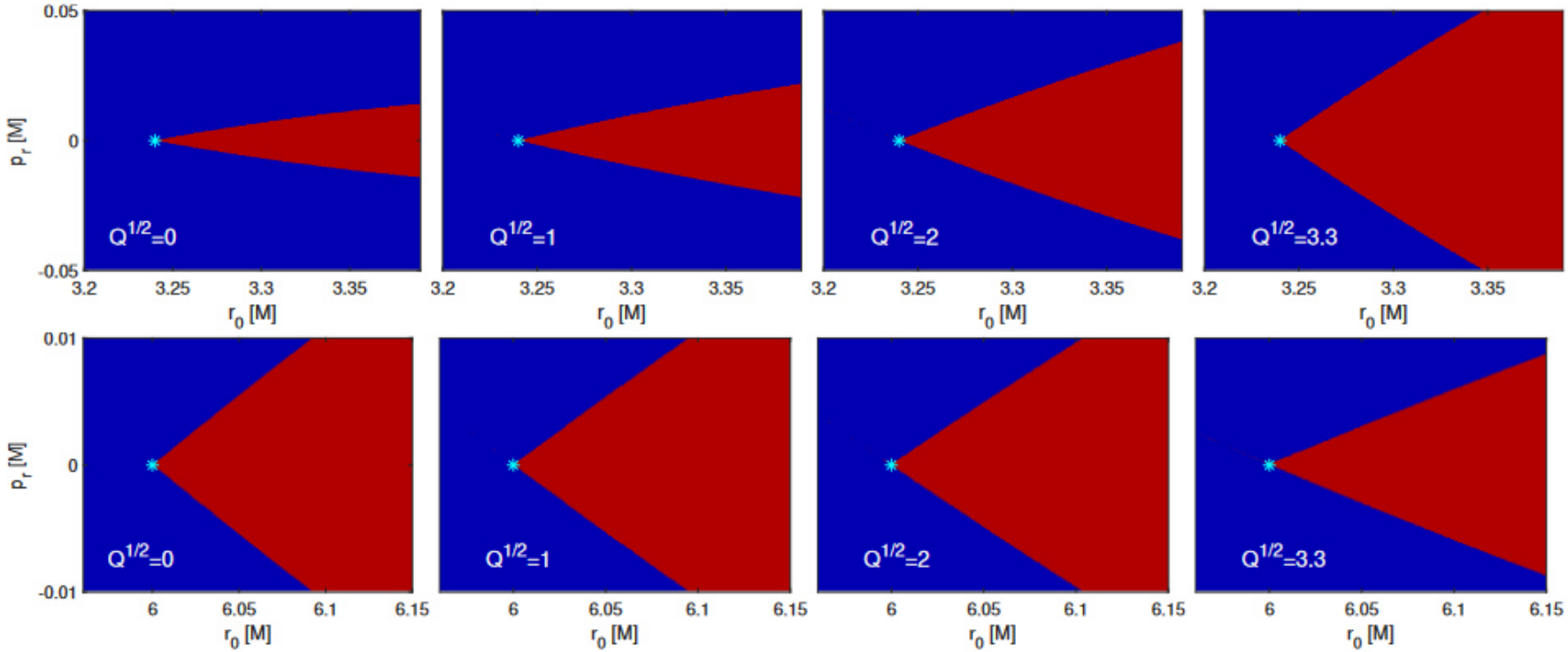

Figure 17. Effect of the Carter constant on the dynamics near unstable spherical orbits (marked by light-blue asterisks in the plots) located between MBSO and ISSO radii. The upper row shows the co-rotating orbits near the unstable orbit at $r_0 = 3.24$ with spin $a = 0.7$, while the bottom row reveals the counter-rotating orbits around unstable orbit $r_0 = 6$ with the spin $a = 0.8$. The range of p_r values (vertical axis) is different in each row in order to make the effect of $Q^{1/2}$ more apparent.

Dynamics between MBSO and ISSO

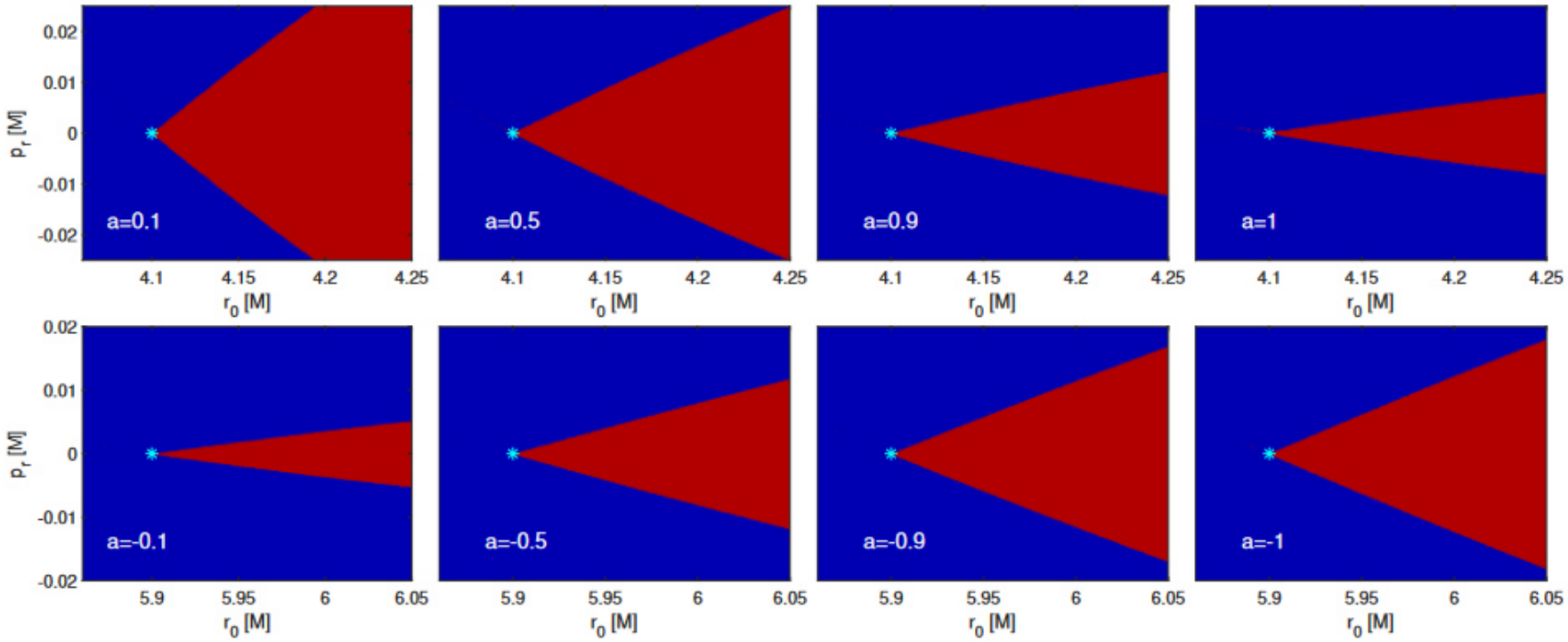

Figure 18. Effect of the spin parameter on the dynamics near unstable spherical orbits (marked by blue asterisks in the plots) located between MBSO and ISSO radii. The upper row shows the co-rotating orbits near the unstable orbit at $r_0 = 4.1$, with $Q^{1/2} = 3$, while the bottom row reveals the counter-rotating orbits around the unstable orbit at $r_0 = 5.9$ with $Q^{1/2} = 1.8$.

Unstable spherical orbits below MBSO

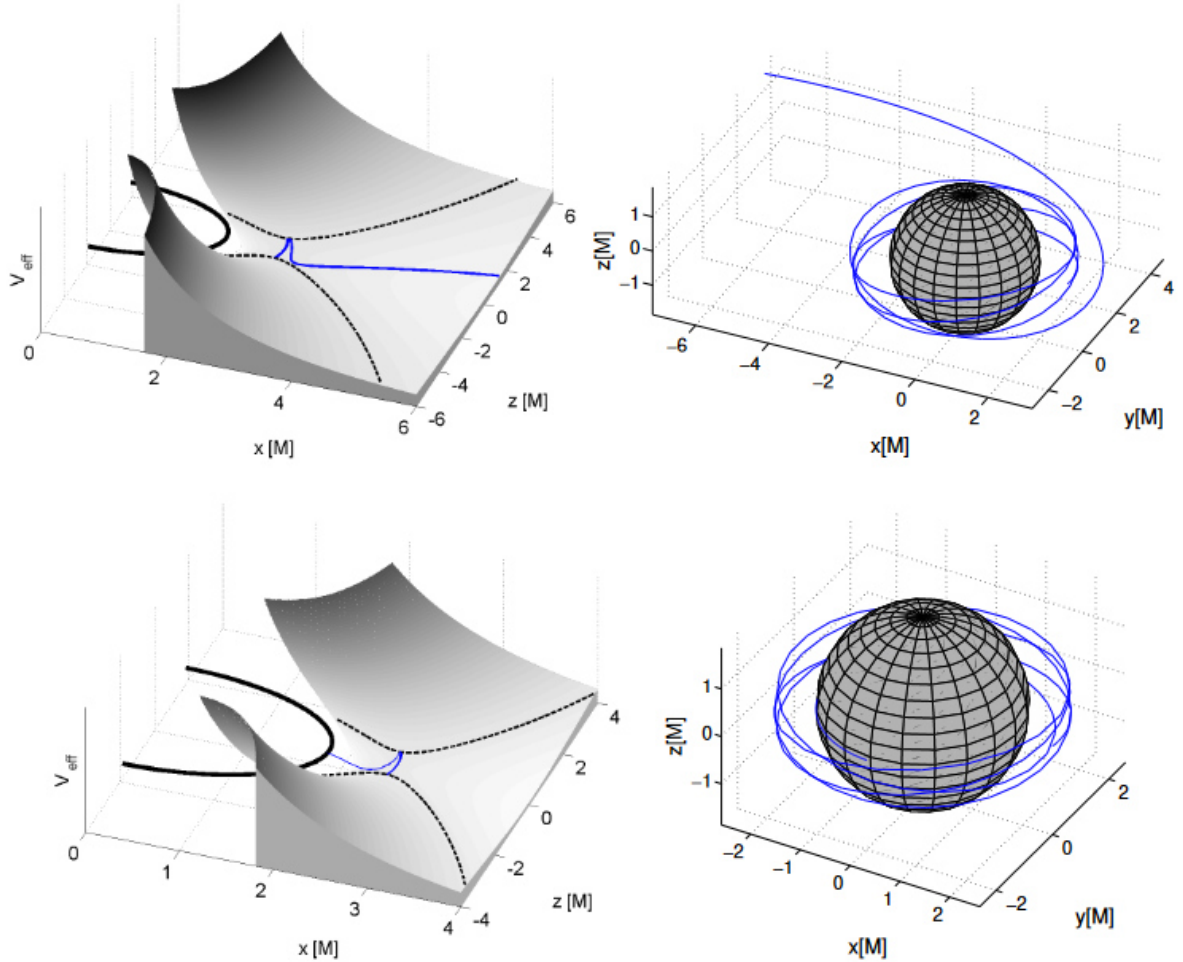

Figure 12. Examples of unstable spherical trajectories below MBSO. Upper row: escaping particle launched from $r_0 = 2.8$. Bottom row: plunging particle launched from $r_0 = 2.6$. Same parameters as in Figs. 10 and 11 are used.

Dynamics below MBSO

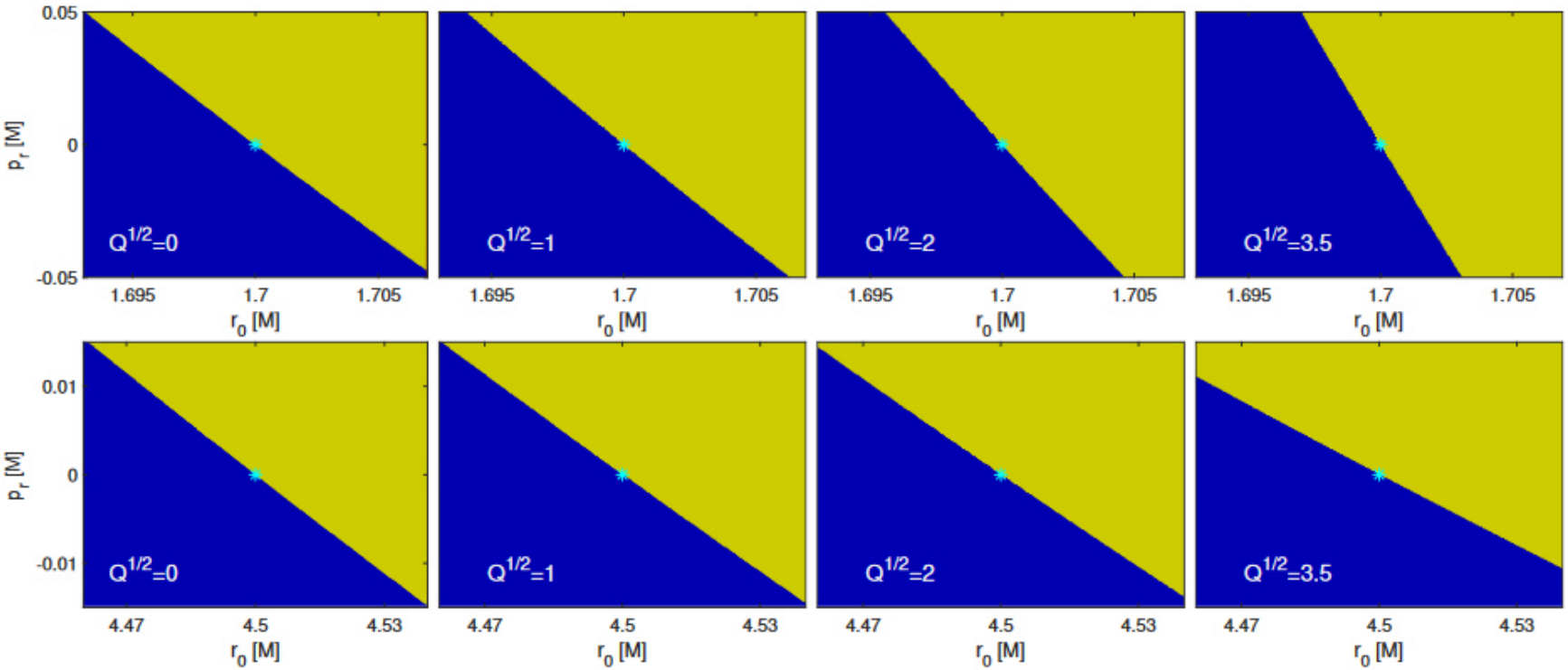

Figure 19. The effect of the Carter constant on the dynamics near unstable spherical orbits (marked by blue asterisks in the plots) that are located below MBSO radius. The upper row shows co-rotating orbits near the unstable orbit at $r_0 = 1.7$ for the spin $a = 0.9$. The bottom row reveals the counter-rotating orbits around the unstable orbit $r_0 = 4.5$ with the spin $a = 0.6$. Note that the range of p_r values (vertical axis) is different in each row.

Conclusions

- **Spherical orbits of massive particles in Kerr spacetime** are a special class of timelike geodesics defined by constant radii. At given radii, spherical orbits are specified by **two parameters**. We used parametrizations by **spin and Carter constant, or** by **spin and turning angle** $\theta_\star$.
- We discussed the radii of the **Innermost Stable Spherical Orbit** (ISSO) and the **Marginally Bound Spherical Orbit** (MBSO). For **co-rotating** orbits, both ISSO and MBSO radii are gradually shifted to **higher radii compared to ISCO and MBCO** of the corresponding circular orbit as the Carter constant increases. For **counter-rotating** spherical orbits, **ISSO and MBSO are always smaller than those of circular orbits** and they decrease as the Carter constant grows.
- Spherical orbits **below ISSO** become **unstable**, and the destiny of a particle, i.e., whether it **plunges** to the black hole, **stabilizes** on a quasiperiodic orbit, or **escapes** (from below MBSO), depends primarily on the phase-space direction of the **perturbation**.
- Assuming that the **perturbation** has a **random** direction in the (r, p_r) plane, we conclude that for particles **between MBSO and ISSO**, the **spin** parameter **decreases the probability of the stabilization for co-rotating orbits** while it **increases this probability for counter-rotating orbits**. The **Carter constant** has an opposite role: it **contributes to the stabilization of co-rotating orbits** while it makes **counter-rotating orbits more prone to plunge**.
- **Below** the **MBSO** radii, the nature of the instability changes to **unstable node** for which the **probability of plunge or escape does not change** with these parameters since the separatrix remains a straight line that only slightly rotates as the spin or Carter constant increases.

Spherical photon orbits in Kerr spacetime

- Teo, E. (2003), Spherical Photon Orbits Around a Kerr Black Hole, General Relativity and Gravitation, 35, 1909.
- Always unstable against radial perturbations.
- Unlike massive particles, spherical photon orbits are obtained as a one-parameter family of orbits, i.e., for a given black hole spin a the orbit is fully defined by radius r.
- For null geodesics described by integrals E, L and Q, only the two ratios $\phi \equiv L/E$ and $\eta \equiv Q/E^2$ are really independent:

$$\phi = -\frac{r^3 - 3r^2 + a^2 r + a^2}{a\,(r-1)}, \qquad \eta = -\frac{r^3\left(r^3 - 6r^2 + 9r - 4a^2\right)}{a^2\,(r-1)^2}. \tag{1}$$

- Only allowed in the range of radii $r_1 \leq r \leq r_2$, where $r_{1,2} = 2\left\{1 + \cos\left[\frac{2}{3}\arccos\left(\mp a\right)\right]\right\}$ are the radii of unstable circular photon orbits in the equatorial plane with $\eta = 0$. Radius r_1 corresponds to a co-rotating orbit while at r_2 we get a counter-rotating circular orbit. The radial range between r_1 and r_2 is divided by an intermediate radius $r_3 = 1 + 2\sqrt{1 - \frac{a^2}{3}}\cos\left(\frac{1}{3}\arccos\frac{(1-a^2)}{(1-\frac{a^2}{3})^{\frac{3}{2}}}\right)$ of the polar orbit with $\phi = 0$.

Off-equatorial orbits

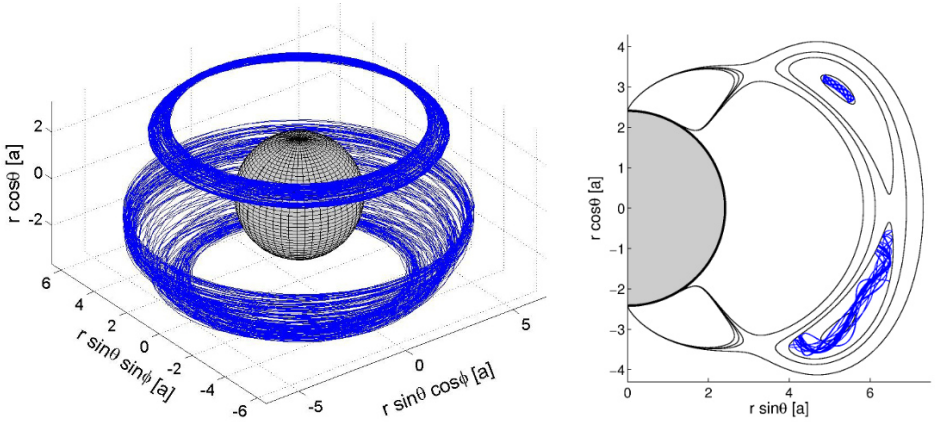

- Timelike orbits of constant radial and latitudinal coordinates located outside the equatorial plane (nonequatorial circular orbits).
- No stable off-equatorial orbits of charged particles are found outside the outer horizon of the Kerr-Newman BH.
- Allowed for charged particles around (weakly) magnetized Kerr black hole (Wald's solution) or massive magnetic dipole (Bonnor's solution); non-integrable systems with chaotic dynamics.
- Kopáček, O., Karas, V., Kovář, J., & Stuchlík, Z. (**2010**), Transition from Regular to Chaotic Circulation in Magnetized Coronae near Compact Objects, The Astrophysical Journal, 722, 1240.
- Kovář, J., Kopáček, O., Karas, V., & Kojima, Y. (**2013**), Regular and chaotic orbits near a massive magnetic dipole, Classical and Quantum Gravity, 30, 025010.

Numerical analysis of unstable dynamics

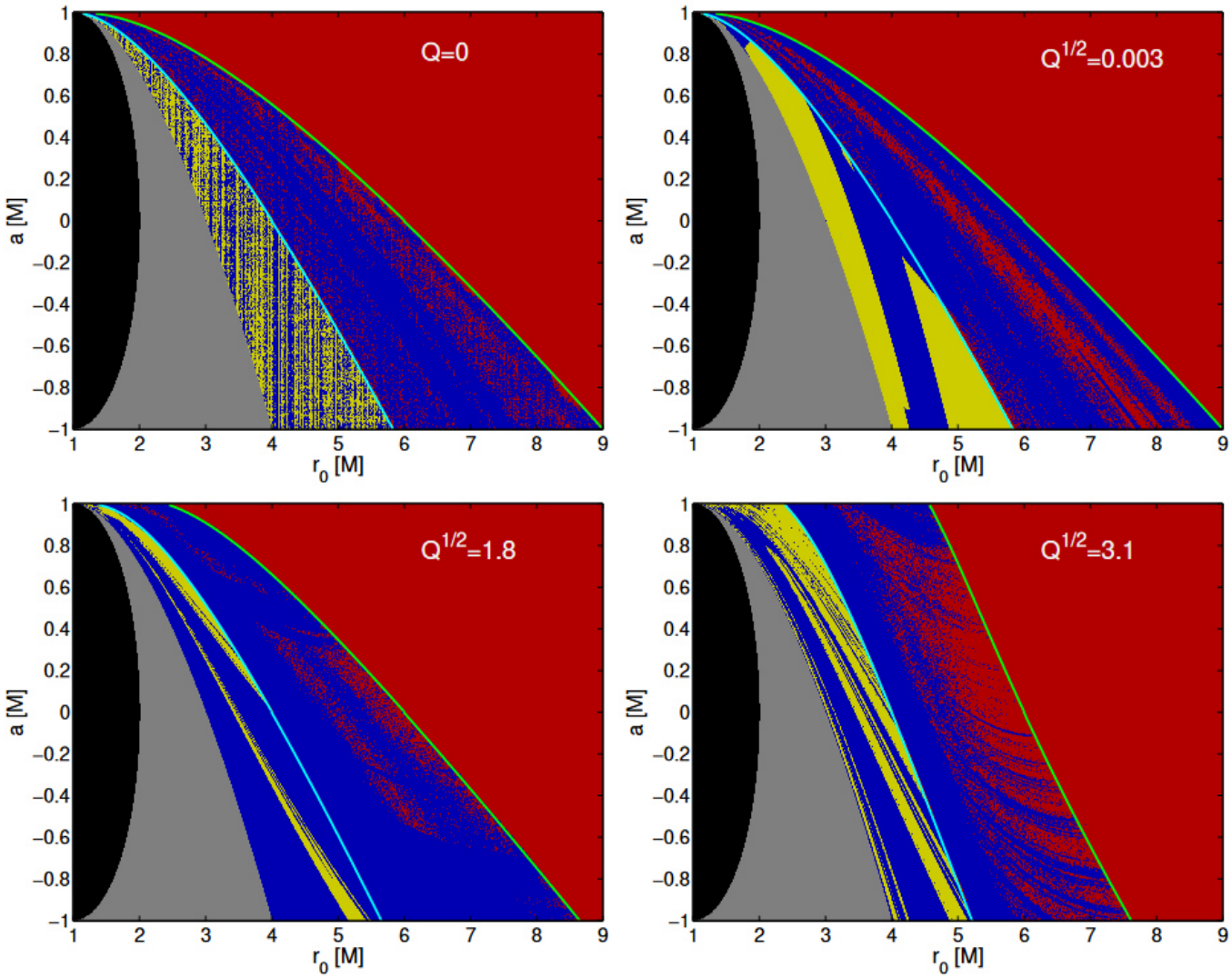

Numerical analysis of unstable dynamics